

## The prophylactic effects of naringin on steroid-induced early-stage osteonecrosis in rats: a preliminary study

Jian Zhuang<sup>1</sup>, Jin Wang<sup>2</sup>, Bingping Zhang<sup>2</sup>, Dongpo Chai<sup>3</sup>, Zhenbo Zuo<sup>2\*</sup><sup>1</sup>Department of Sports Medicine, Qilu Hospital (Qingdao), Cheeloo College of Medicine, Shandong University, Qingdao, Shandong 266035, China<sup>2</sup>Department of Orthopaedics, Affiliated Hospital of Qingdao University, Qingdao, Shandong 266003, China<sup>3</sup>Department of Orthopaedics, Huikang Hospital of Qingdao, Qingdao, Shandong 266400, China

### ARTICLE INFO

#### Original paper

#### Article history:

Received: February 03, 2023

Accepted: May 07, 2023

Published: May 31, 2023

#### Keywords:

BMP (bone morphogenetic protein), gene expression, osteogenesis, PPAR $\gamma$ 2 (peroxisome proliferator-activated receptor gamma 2), RT-qPCR (quantitative real-time reverse transcription polymerase chain reaction)

### ABSTRACT

The excessive steroid may cause dyslipidaemia and oxidative insult during femoral head osteonecrosis, inducing bone loss and impairment of the intraosseous blood system. In contrast, bio-flavanone naringin has shown antioxidant, antiresorptive and lipid-lowering bioactivities. The present research is an effort to explore the anti-ON potential of naringin *in vivo* and *in vitro*. After a 6-week treatment, the femora were dissected for histological examination following bone mineral density assay by X-ray absorptiometry. Blood samples were examined for coagulation, oxidative stress, lipid transportation and endothelial injury. Marrow samples were cultured and assayed for adipogenic and osteogenic alterations by ALP activity, mineralization, RT-qPCR and western blot analysis. The results showed that naringin exerted a dose-dependent effect on reducing ON incidence, with inhibition of osteoporosis, oxidative stress and dyslipidaemia. The mechanism included the suppression of PPAR $\gamma$ 2 for adipogenesis of bone marrow stem cells (BMSCs) and the prevention of oxidative stress in endothelium injury. Naringin may restore steroid-impaired osteogenesis by enhancing the mRNA and protein expression of osteogenic markers in a dose-ascending manner and new bone formation can be found in naringin groups. Taken together, our findings showed that naringin may serve as a prophylactic agent and selective PPAR $\gamma$  modulator for the early-stage ON.

Doi: <http://dx.doi.org/10.14715/cmb/2023.69.5.16>Copyright: © 2023 by the C.M.B. Association. All rights reserved. 

### Introduction

With the worldwide outbreak of 2019-nCoV, pulsed steroids are frequently prescribed as a life-saving agent for severe 2019-nCoV pneumonia. But steroid-induced osteonecrosis of the femoral head (SONFH) should be kept in mind because it often disables the young population aged 30-50 years (1). Statistically, more than 80% of ONFH patients may progress to collapse and secondary hip arthritis without any intervention (2), which results in final hip dysfunction (3). Recent surveys have indicated that ONFH afflicts more than 20 million people worldwide, 5-7.5 million in China (4). Excessive steroid use is the most common cause of osteonecrosis (ON) and makes up 24.4%-51% of total ONFH cases (5). The ON incidence in steroid users may reach 40%, depending on the duration, dose or underlying disease (6). Notably, in China, 53.5% of steroid users with severe acute respiratory syndrome developed ONFH (7). But the etiology of steroid-induced ONFH (SONFH) remains controversial and various theories explain it, including hyperlipidaemia, coagulation abnormalities, oxidative stress and osteoporosis theory (3, 7-9). Mont et al. (1) reported that fat embolism, vascular thrombi, osteocyte and osteoblast apoptosis, and oxidative stress played a key role in SONFH. Extra-

vascularly, the substantial lipid transportation to periphe-  
ral tissue and adipocyte hypertrophy led to intraosseous  
hypertension (10,11), thereby inhibiting blood perfusion  
even to ischemia. Intravascularly, hyperlipidaemia and  
oxidative stress-induced endothelium injury consistently  
caused predisposition to both hypercoagulation and hypo-  
fibrinolysis, imparting the thrombi or fat emboli even to  
vascular occlusion (12,13). Due to the progressive ische-  
mia, reparative osteocytic necrosis and apoptosis may  
result in structural bone weakening and osteoporosis (14-  
17). Elevated adipogenesis of bone marrow stromal cells  
(BMSCs) via PPAR $\gamma$ 2 overexpression may further lessen  
trabecular mineral density, leading to subchondral col-  
lapse (15-18).

Unfortunately, most patients need total hip arthro-  
plasty (THA) within a few years of collapse eventually.  
As prosthetic longevity is limited, they have to face the  
psychological and economic burdens of revised arthro-  
plasty. Thus, THA is not the optimal treatment for a rela-  
tively young population (19). Although surgical options  
including core decompression (CD) (20,21), multiple drill-  
ing (22,23), osteotomy (24,25), and CD combined with  
adjunctive procedures (26-29) may relieve symptoms and  
postpone THA, more investigations and long-term results  
are needed to confirm the efficacy of these approaches

\* Corresponding author. Email: [wave\\_zuo@yeah.net](mailto:wave_zuo@yeah.net)

(1,30). Notably, many nonsurgical strategies, such as pharmacological agents (lipid-lowering agents, anticoagulants, vasoactive substances, and bisphosphonates) and biophysical modalities (extracorporeal shockwave therapy, pulse electromagnetic therapy, and hyperbaric oxygen therapy) may help prevent further bone deterioration at the early stage (31). However, these therapies are still controversial and lack sufficient evidence for widespread use (31,32). Bisphosphonates (BPs) are the most widely used agents in treating ON, but cause many side effects that offset their benefits, including atypical femoral fracture, esophageal cancer and renal dysfunction (33). Given the complex pathogenesis, the ideal strategy should be to simultaneously target the above mechanisms and salvage the femoral head at the early stage with minimal toxicity.

Epidemiological data have shown that there was a lower prevalence (5-6%) of ON in SARS patients recovered from steroid use who simultaneously accepted the crude flavonoid extracts of Chinese herbs in southern China, whereas there was a higher prevalence (32.7%) of ON patients who have seldom prescribed the natural products in northern China (34). Therefore, natural products have been found to hold remarkable potential for the development of new drugs. Naringin (Nar) is a polymethoxylated flavonoid commonly found in citrus fruits and many Chinese herbs. Accumulating evidences have shown that naringin may enhance osteoblast proliferation and differentiation by increasing the expression of osteogenic markers such as osteocalcin (OCN), osteopontin (OPN), osteoprotegerin (OPG) and bone morphogenetic protein-2 (BMP-2) mediated by PI3K-Akt, c-Fos/c-Jun and AP-1 pathway (35). Its osteo-protective role displays multiple biological actions including antioxidant, antiapoptotic, vasculogenic, hypolipidaemic and antiosteoporotic properties (36). Naringin can protect against oxidative insults and promote osteoblast maturation by regulating osteogenic expression (37). Kandhare reported that naringin has anti-apoptotic properties and stimulated angiogenesis in wound tissue (38). Naringin enhanced endothelial progenitor cell proliferation and tube formation capacity by the CXCL12/CXCR4/PI3K/ Akt signal pathway (39). Furthermore, naringin was reported to influence oxidative stability and lower lipid profile by inhibiting the hydroxymethylglutaryl coenzyme A (HMG-CoA) reductase activity on the mevalonate pathway in cholesterol production (40). As a lipid-lowering agent, naringin had a similar effect to statins in the simultaneous activation of BMP-2 by HMG-CoA reductase inhibition (40). Meantime, naringin showed an estrogenic protective effect against osteoporosis and abrogated osteoclast-mediated bone resorption via impeding RANKL-induced NF- $\kappa$ B and ERK activation (33,41). However, little is known about its prophylactic effect on SONFH. Hence, our study was aimed at examining its multiple regulatory effects on the rat ON.

## Materials and Methods

### Animals and treatment

A total of 73 male 5-month-old Sprague-Dawley rats of 300-350g in weight were purchased from the Laboratory Animal Centre of Qingdao University (Qingdao, China) and maintained on a standard diet and water. The procedures followed the National Science Academy Guidelines for the use and care of experimental animals and

were approved by the Animal Care and Use Committee of Qingdao University. According to Qin's protocol with modifications (42): 1mg/kg lipopolysaccharide (LPS, Sigma Aldrich) was injected through the tail vein to induce bone necrosis, and this process was repeated after 24 h. Following the second LPS, three injections of 20 mg/kg methylprednisolone (MPS, Pfizer Pharmaceutical, China) were given intramuscularly at intervals of 24 h. The rats accepting the ON induction were randomly divided into 3 daily gavage groups: a low-dose group (L-Nar, n=19; 300 mg/kg/d), a high-dose group (H-Nar, n=19; 600 mg/kg/d), and a model group orally treated with distilled water (MOD, n=19). The naringin dosage was adopted based on the other studies (40,43). The remaining 13 rats were used as the control group and received distilled water orally (CON, n=16). All rats were euthanized 6 weeks after the MPS injection for further evaluations. It was reported that ON gradually developed 6 weeks after MPS injection, and was equivalent to Stage II ON clinically (Ficat and Arlet classification system) (42). The animal weight and survival condition were recorded weekly for adjusting the naringin dosage. Naringin (chemical purity>98%) was purchased from Xi'an Guanyu Bio-tech company (Xi'an, China).

### Haematological assay

Blood samples were obtained from the fasting rats for examination of the coagulation index (APTT, i.e., activated partial thromboplastin time), fibrinolysis index (t-PA/PAI-I, i.e., ratio of tissue plasminogen activator to plasminogen activator inhibitor), lipid transportation index (LDL/HDL, i.e., ratio of low-density lipoprotein to high-density lipoprotein), endothelium injury index (TM, i.e., thrombomodulin) (44), oxidative stress index (GSH/LPO, i.e., the ratio of glutathione to lipid peroxide) (45) and hepatotoxicity index (GPT, i.e., glutamate-pyruvate transaminase) (46) at week 0 (immediately before LPS injection), 1, 2, 4 and 6 post-induction.

### Bone mineral density (BMD) measurements

At week 6, the BMD of the legs ( $\text{g}/\text{cm}^2$ ) in each group was measured in vivo by dual-energy X-ray absorptiometry (DXA; Lunar-Prodigy, GE Healthcare, USA) using the small animal mode as reported elsewhere (47,48). The scanner was calibrated daily against the standard calibration block supplied by the manufacturer to control for possible baseline drift. Prior to scanning the rats were anesthetized with dexmedetomidine (300 $\mu\text{g}/\text{kg}$ , ip) and supine on a DXA table with hind limbs flexed and extorsion. The femur was divided into three regions of interest (ROIs) as previously described (49): proximal ( $r_1$ ) and distal ( $r_2$ ) metaphysis with diaphysis ( $r_3$ ). All of the scans were performed by the same trained technician, and all the data were sampled three times.

### Histopathological examination

After sacrifice, bilateral femurs were fixed in 10% neutral buffered formalin, decalcified with 10% ethylene diamine tetraacetic acid (EDTA)-0.1 M phosphate buffer (pH 7.4) and embedded in paraffin. The specimens were coronally cut into 5- $\mu\text{m}$  thick slices and stained with hematoxylin-eosin (H&E). All the slices from each group were examined for ON presence and repair process under a light microscope (Olympus Corporation, Tokyo, Japan) at a magnification of 200. Each rat that had at least one

ON lesion, i.e. the presence of empty lacunae or pyknotic nuclei of osteocytes in the trabeculae accompanied by surrounding necrotic bone marrow was defined as ON<sup>+</sup>, while the rat without ON lesion was identified as ON<sup>-</sup> (50). For each group, ON incidence was calculated as the number of ON<sup>+</sup> rats divided by the total in each group. Its location was evaluated in the diaphysis and metaphysis. The extent of ON was determined by the number of ON lesions per ON<sup>+</sup> rat. To further investigate ON amelioration by naringin treatment, new bone fraction and microvessel density in ON lesions were measured using Image-Pro Plus 6.0 software (Media Cybernetics, Bethesda, MD). The new bone fraction was defined as the ratio of the new bone area to the total focal area  $\times 100$ , while microvessel density was calculated as the microvessel numbers divided by the total focal area. Osteoid tissue was excluded from the new bone calculation as the inclusion of osteoid tissue may lead to overestimation.

Marrow adipocytes were quantitatively measured in eight randomly selected fields (one field =  $25 \times 10^{-8} \text{m}^2$ ) of each section from each rat with Image-Pro Plus 6.0 software (Media Cybernetics, Bethesda, MD) according to the method as described previously (48). Mean adipocyte diameter ( $\mu\text{m}$ ), adipocyte density (number/ $\text{mm}^2$ ), and percentage of adipocyte volume per marrow volume (Ad.V/Ma.V; %) were processed automatically by the computer system. Adipocyte necrosis was excluded and the experiments were performed in triplicate.

#### Rat BMSC culture

Rat BMSCs were isolated and cultured at week 6 according to the protocol reported previously (40). Briefly, both ends of the femurs from 4 groups were cut off at the epiphysis, and the marrow was aspirated with 10 ml low-glucose Dulbecco's Modified Eagle's medium (LG-DMEM; Invitrogen, Carlsbad, CA, USA) containing 10% fetal bovine serum (FBS) and antibiotics (100 U penicillin and 100 mg/ml streptomycin) by using a needle and syringe (18-gauge). BMSCs were separated by density gradient centrifugation, plated at  $1 \times 10^6$  cells/ml in 25 ml cell culture flasks and incubated in 5%  $\text{CO}_2$  at 37°C. After 3 days, the culture medium and non-adherent cells were removed. The medium was changed two or three times a week. Until 80% confluence was attained, cells (prior to passage 5) were subcultured or plated for subsequent experiments.

#### Alkaline phosphatase (ALP) activity and mineralization assay

To address whether naringin may reverse the osteogenesis of ON-derived BMSCs, ALP activity and calcium deposits were assayed after cytochemical staining (16,40,43,51). Firstly, cells from each group were seeded at  $1 \times 10^5$  cells/ml in 6-well plates to reach 80% confluence and cultured in the osteogenic induction medium (OIM: 10% FBS, 10 mM  $\beta$ -glycerophosphate sodium, 0.1  $\mu\text{M}$  dexamethasone, and 50  $\mu\text{M}$  ascorbic acid). After incubation for 2 and 3 weeks, cells were washed twice in PBS and set in 100% ethanol for 15 minutes. ALP and Alizarin red S (AR-S) staining were accomplished using a relevant kit (Renbao, Shanghai, China) as per the manufacturers' instructions, and stained cells were photographed using an Olympus digital camera.

For the ALP activity assay, cells were rinsed twice with

PBS and scraped into a lysis solution containing 10 mM Tris-HCl (pH 7.4), 0.1% Triton X-100 and 0.5 mM  $\text{MgCl}_2$ . Each lysate was sonicated and centrifuged at  $13,000 \times g$  for 3 min at 4°C. The supernatants were subjected to ALP activity and protein content measurements using an ALP assay kit (Nanjing Jiancheng Biotech, China) and a BCA assay kit (Sangon, China), respectively. The optical density at 405 nm was measured on a microplate reader. ALP activity was calculated using a p-nitrophenol standard curve and expressed as U/ml per mg protein. For the mineralization assay, the cultures were rinsed five times with deionized water and once with PBS for 15 min to reduce nonspecific AR-S staining. Calcium nodules were quantified by desorbing AR-S stain with 10% cetylpyridinium chloride (CPC, Sigma-Aldrich, St. Louis, Mo. USA) for 1 h at room temperature. The absorbance of the extracted AR-S stain was measured at 562 nm spectroscopically. AR-S concentrations were determined by comparison with an AR-S dye standard curve and expressed as nmol/ml. Finally, ALP and AR-S levels were normalized to the total protein content across treatments. All experiments were conducted in triplicate.

#### Quantitative RT-PCR (RT-qPCR) and Western blot analysis

For assessing its capability to abolish the suppression of osteogenesis, RT-qPCR was employed for detecting BMP-2 (bone morphogenetic protein-2), Runx2 (run-related transcription factor 2), OCN (osteocalcin), OPN (osteopontin), ALP (alkaline phosphatase) and PPAR $\gamma$ 2 (peroxisome proliferator-activated receptor gamma 2) expression of ON-derived BMSCs at week 6 post-induction (16,52,53). Briefly, cells were lysed and homogenized with 1 ml of Trizol reagent (Invitrogen, USA), added to 200  $\mu\text{l}$  of chloroform, and centrifuged at 12,000 rpm for 15 minutes. The RNA pellets were washed with 75% ethanol, dried, and dissolved in RNase-free water. Quantity and quality of RNA were assessed by absorbance at 260/280 nm and agarose gel electrophoresis. Aliquots of RNA samples (2  $\mu\text{g}$ ) were subjected to first-strand cDNA synthesis using 100 units of M-MLV reverse transcriptase (Fermentas, USA) per reaction with an oligo-dT primer (Promega, USA), and 0.5  $\mu\text{l}$  cDNA solution was then for gene-specific PCR on a Bio-Rad iQ5 thermal cycler (Applied Biosystems, USA) using a cDNA template, specific primers, and SYBR Green supermix (Takara, Japan) in a total volume of 20  $\mu\text{L}$ . PCR was carried out for 40 cycles of initial denaturing (94°C, 4min), annealing (94°C, 30s), and extension (56°C, 60s) with a final extension at 72°C for 40s. The primers were synthesized commercially (Shengong Co. Ltd., Shanghai, China) and the details are listed in Table 1. Glyceraldehyde-3-phosphate dehydrogenase (GAPDH) served as a housekeeping gene. The relative amounts of each gene mRNA expression to GAPDH were measured with the SYBR® Premix Ex Taq™ (Takara, Japan). The fold change of mRNA expression was calculated as  $2^{-\Delta\Delta\text{Ct}}$ , where  $\Delta\Delta\text{Ct} = \Delta\text{Ct}_{\text{treatment}} - \Delta\text{Ct}_{\text{vehicle}}$  and  $\Delta\text{Ct} = \text{Ct}_{\text{target gene}} - \text{Ct}_{\text{GAPDH}}$ .

To detect the protein expression of osteogenic or adipogenic markers, cells were first homogenized on ice in a lysis buffer containing PMSF (Beyotime, China) for 0.5 h (16,52,53). Following centrifugation at 10,000 rpm for 10 min at 4°C, equal amounts of total protein (50  $\mu\text{g}$ ) from the supernatant were separated by 10% sodium dodecyl

**Table 1.** Primer sequences for BMP-2, Runx2, OCN, OPN, ALP, PPAR- $\gamma$  and GAPDH.

| Gene           | Sequence                   |                              | Size (bp) |
|----------------|----------------------------|------------------------------|-----------|
|                | Forward primer             | Reverse primer               |           |
| BMP-2          | 5' GGGTGAATGACTGGATCG 3'   | 5' ACTATGGCATGGTTGGTGGGA 3'  | 110       |
| Runx2          | 5' CAGACCAGCAGCACTCCAT 3'  | 5' CCATCAGCGTCAACACCA 3'     | 182       |
| OCN            | 5' GACCACATTGGCTTCCAG 3'   | 5' GTGCCGTCCATACTTTCG 3'     | 157       |
| OPN            | 5' AGCCAGCCTGGAACATCA 3'   | 5' TGCCTCTTCTTTAATTGACCTC 3' | 152       |
| ALP            | 5' CCCACAAGAGCCCACAATG 3'  | 5' GGAAGTGAGGCAGGTAGCAAA 3'  | 128       |
| PPAR- $\gamma$ | 5' CAGACCTCAGGCAGATTGTC 3' | 5' TTTGTCAGCGACTGGGAC 3'     | 141       |
| GAPDH          | 5' TCAAGAAGGTGGTGAAGCAG 3' | 5' AAGGTGGAAGAATGGGAGTT 3'   | 112       |

sulfate-polyacrylamide gel electrophoresis (SDS-PAGE) and then transferred to nitrocellulose membranes. Next, membranes were blocked with 5% nonfat milk in TBS/Tween 20 (TBST) for 1 h at 37°C, and probed with the following primary antibodies overnight at 4°C: mouse monoclonal anti-GAPDH, anti-Runx2, anti-ALP, anti-BMP2, anti-OCN, anti-OPN and anti-PPAR $\gamma$ 2. Finally, cells were incubated with a horseradish peroxidase-conjugated secondary antibody for 1 h at room temperature. GAPDH was used as a loading control. Protein bands were visualized by an enhanced chemiluminescence (ECL) system (Thermo Fisher Scientific Inc. USA). All experiments were performed in triplicate.

**Statistical analysis**

All data were expressed as the mean $\pm$ SD and entered into SPSS18.0 (SPSS, Inc., Chicago, IL). In the event of statistical significance at  $P < 0.05$ , ANOVA of repeated measures was performed to compare marrow molecular, cytological, and ON extent in each group using LSD's post hoc multiple comparisons. BMD, haematological and histopathological data were analyzed by GLM (General Linear Model)-based univariate analysis of variance with body weight as the covariate to eliminate its influence on the results. ON incidence in each group was analyzed using Fisher's exact probability test. Pearson correlation coefficients were used for seeking the reciprocal association of these factors.

**Results**

**Safety evaluation and prevention efficacy**

One rat in the MOD died of pneumonia due to endotoxin shock and the others showed reduced activities and food intake with increased shedding and diarrhea than Nar-fed animals. Figure 1A showed that LPS induced the lowest body weight at week 1 and recovered slowly but still lower than the CON ( $P < 0.05$ ). The chronic feeding of

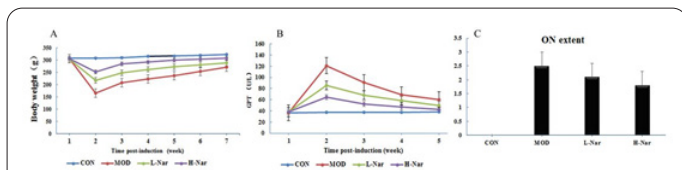


**Figure 1.** Comparisons of body weight, GPT or ON extent among 4 groups. The most conspicuous early signs of LPS-induced weight loss and GPT increase occurred at week 1 post-induction, but Nar could reverse these vicious changes in a dose-related manner and almost restore to the normal level (A, B). As a whole, ON extent did not vary significantly among 3 groups (C,  $P > 0.05$ ).

Nar attenuated the LPS-induced tendency of weight loss across the time points as compared to the MOD ( $P < 0.05$ ). Figure 1B showed that the GPT level in the CON and Nar-fed groups was similar ( $P > 0.05$ ), but LPS induced a 3-fold GPT increase in MOD at week 1 and this elevation lowered gradually, still higher than in other groups at each time point ( $P < 0.05$ ). The incidence of ON in the MOD (17/18, 94.4%) was significantly higher than in L-Nar (12/19, 63.2%) and H-Nar (5/19, 26.3%) groups ( $P = 0.001$  for both). ON occurrence was lower in the H-Nar group than in the L-Nar group ( $P = 0.049$ ). ON lesions were mainly focused on the proximal and distal metaphysis, and the extent of ON did not vary significantly among the MOD ( $2.5 \pm 0.8$ ), L-Nar ( $2.1 \pm 0.9$ ) and H-Nar groups ( $1.8 \pm 0.4$ ) ( $P = 0.143$ , Figure 1C).

**BMD and histopathological data**

When exposed to Nar at 300mg/kg and 600mg/kg for 6 weeks, DXA analysis showed a clear decrease of BMD in the metaphyses ( $r_1$  and  $r_2$ ) of MOD compared with the CON (Figure 2A,  $P < 0.01$ ), while naringin treatment in-

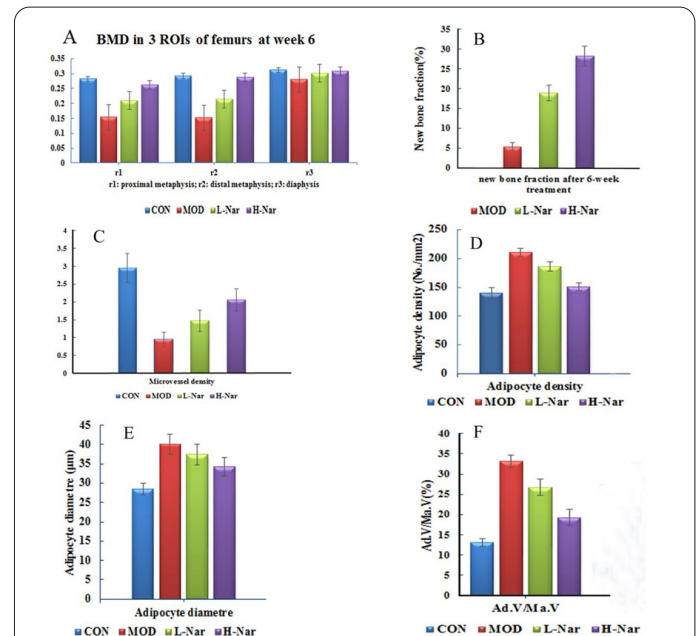


**Figure 2.** A. Nar and MPS induced the obvious BMD changes in  $r_1$  and  $r_2$  ( $P < 0.01$ ), but no significant changes in  $r_3$  were observed among 4 groups ( $P > 0.05$ ). Nar treatment induced a gradual increase in the metaphyses with the ascending doses among 2 groups compared with the MOD ( $P < 0.01$ ). B and C: Due to its antiresorptive and vasculogenic actions, new bone fraction and microvessel density were raised in 2 Nar-fed groups ( $P < 0.01$ ). D-F: L-Nar and H-Nar decreased the adipocyte parameters (density, diameter and Ad.V/Ma.V) compared to the MOD ( $P < 0.05$ ), respectively.

duced a gradual increase in the metaphyses with the ascending doses among 2 groups compared with the MOD ( $P < 0.01$ ). BMD in the metaphyses of the L-Nar group and  $r_1$  in the H-Nar group was still lower than in the CON group ( $P < 0.05$ ), while  $r_2$  in the H-Nar group was similar to the CON group ( $P > 0.05$ ). However, no significant changes in  $r_3$  were observed among the 4 groups ( $P > 0.05$ ), indicating that naringin had a site-specific effect on BMD improvement of femoral epiphyses. Bone changes were also confirmed by histological examination.

After 6-week treatment, neither subchondral bone nor intraosseous collapse was observed in ON<sup>+</sup> samples. ON lesions in the MOD showed empty lacunae or pyknotic nuclei of osteocytes in sparser trabeculae and adipocyte hyperplasia in the medulla (Figure 3A, B). In 2 Nar-fed groups, empty lacunae and pyknotic nuclei of osteocytes were lessened, but the trabecular number and volume increased. The penetration of capillaries and osteocytes and the reparative response resulted in the appositional bone formation surrounding necrotic foci or granulation tissue moving from adjacent viable tissue to the dead bone (Figure 3C-F). The H&E staining showed that the new bone fraction was significantly higher in H-Nar than in the other 2 groups at week 6 ( $P < 0.01$ , Figure 2B). Accordingly, microvessel density in MOD was  $0.95 \pm 0.43$  vessels/mm<sup>2</sup> which was obviously lower than that in H-Nar ( $1.93 \pm 0.52$  vessels/mm<sup>2</sup>) and L-Nar ( $1.47 \pm 0.49$  vessels/mm<sup>2</sup>), i.e., MOD < L-Nar < H-Nar ( $P < 0.01$ , Figure 2C).

Figure 3A showed that marrow adipocytes with distinct translucent ellipsoids occupied most of the marrow cavity in MOD, whereas fewer adipocytes were embedded in the bed of marrow nuclear cells in the other 2 groups (Figure 3C, E). MOD rats had higher marrow adipocyte density (by 60.9%), diameter (by 40.9%), and Ad.V/Ma.V (by 151.8%) than the CON ( $P < 0.001$  for all). In comparison, adipocyte parameters in H-Nar were smaller than that in L-Nar and MOD, i.e., H-Nar < L-Nar < MOD ( $P < 0.01$ ), but still could not restore to the normal level in CON ( $P < 0.01$ , Figure 2D-F). In 2 Nar-fed groups microvessels, haemorrhage in the medulla and numerous osteoblasts around the necrotic bone was observed due to decreased adipocytes (Figure 3C-F).

**Biochemical assessment**

For lipid transportation, the LDL/HDL ratio showed an obvious increase in MOD at week 1 after the MPS injection and declined towards the normal level (CON) thereafter ( $P < 0.05$ ). However, there was no evident increase in 2 Nar-fed groups after week 1 ( $P < 0.05$  for L-Nar vs MOD and  $P < 0.01$  for H-Nar vs MOD) (Figure 4).

For steroid-induced disturbances of the coagulation-fibrinolysis system, both APTT and t-PA/PAI-I showed a significant decrease in MOD compared to CON at week 1 ( $P < 0.05$  for both) but recovered gradually thereafter. The obvious changes in both t-PA/PAI-I and APTT were attenuated in L-Nar ( $P < 0.05$  for L-Nar vs MOD) and were almost absent in H-Nar ( $P > 0.05$  for H-Nar vs MOD, Figure 4).

For oxidative stress-induced endothelial injury, serum TM increased while GSH/LPO decreased clearly in MOD at week 1 ( $P < 0.01$  for both) and returned to the normal level (CON). The obvious changes in both TM and GSH/LPO were attenuated in L-Nar, while there was almost no change in H-Nar ( $P < 0.05$  for L-Nar vs MOD and  $P < 0.01$

for H-Nar vs MOD, Figure 4).

**Effect of naringin on ALP activity and mineralization of ON-derived BMSCs**

ALP is an early osteogenic differentiation marker, while mineralization or calcium deposit represents the final step

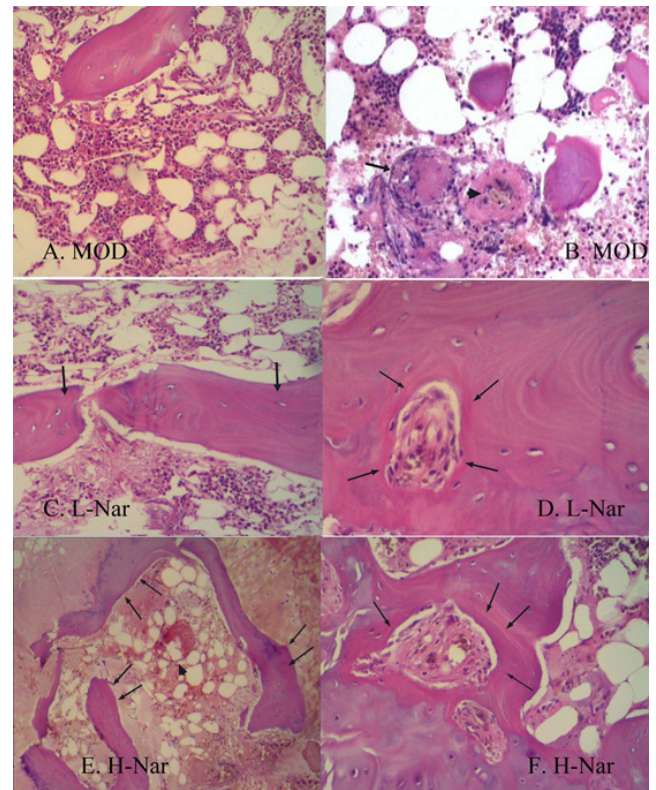


**Figure 3.** H&E staining of the specimens among 3 groups. A: ON lesions in MOD at a magnification of 200 showed empty lacunae or pyknotic nuclei of osteocysts in sparser trabeculae and adipocyte hyperplasia in the medulla with the endothelial injury (pointed by black arrow in B) or thrombi (pointed by arrow head in B) in microvessels at a magnification of 500. In 2 Nar-fed groups (C, E), empty lacunae and pyknotic nuclei of osteocytes were lessened, but the trabecular number and volume increased. Appositional bone formation (pointed by black arrow in C-F) occurred with the penetration of increased capillaries and osteocytes (D, F). Haemorrhage in the medulla and numerous osteoblasts around the necrotic bone were observed due to decreased adipocytes (pointed by arrow head in E).

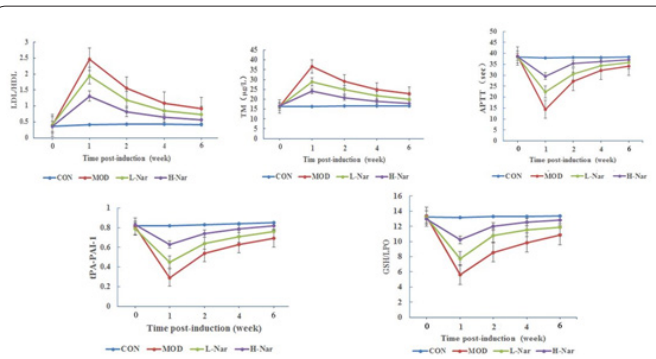


**Figure 4.** Haematological comparisons among 4 groups during 6 weeks. Obviously increased LDL/HDL and TM in MOD at week 1 were attenuated in L-Nar group and prevented in H-Nar group compared with the CON thereafter ( $P < 0.05$ ), whereas significantly decreased APTT, t-PA/PAI-I and GSH/LPO in MOD at week 1 were attenuated in L-Nar group and prevented in H-Nar group compared with the CON thereafter ( $P < 0.05$ ).

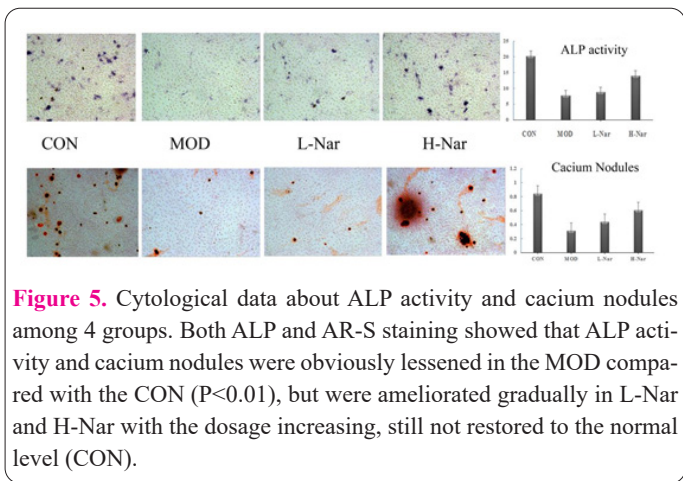


**Figure 5.** Cytological data about ALP activity and calcium nodules among 4 groups. Both ALP and AR-S staining showed that ALP activity and calcium nodules were obviously lessened in the MOD compared with the CON ( $P < 0.01$ ), but were ameliorated gradually in L-Nar and H-Nar with the dosage increasing, still not restored to the normal level (CON).

of osteogenesis. In comparison with MOD, ALP staining from the other 3 groups showed that the areas of positive staining increased proportionally with the dosages ascending (Figure 5). ALP activity showed a similar pattern to ALP staining, indicating that naringin can strengthen the total intracellular synthesis of ALP and abolish the suppression of osteoblastic differentiation in a dose-related manner ( $P < 0.05$  for L-Nar vs MOD and  $P < 0.01$  for H-Nar vs MOD).

The result of AR-S staining showed that there was a greater calcium node formation ratio in the naringin groups than in MOD, but still less than in CON. The dose-related naringin increased the quality and quantity of calcium node formation compared to the MOD ( $P < 0.05$  for L-Nar vs MOD and  $P < 0.01$  for H-Nar vs MOD, Figure 5).

**Effects of naringin on osteogenic and adipogenic gene expression**

The dose-dependent naringin treatment displayed an obvious increase in the osteogenesis-specific BMP-2, Runx2, ALP, OCN and OPN compared with that in MOD ( $P < 0.05$  for L-Nar vs MOD and  $P < 0.01$  for H-Nar vs MOD, Figure 6), whereas naringin inhibited the adipocyte-specific PPAR $\gamma$ 2 to a greater extent in H-Nar than in L-Nar ( $P < 0.05$  for L-Nar vs MOD and  $P < 0.01$  for H-Nar vs MOD, Figure 6). The data revealed that naringin exerted dual influences on BMSCs by promoting osteogenesis and suppressing adipogenesis.

**Effects of naringin on the osteoblast differentiation-related protein expression**

In parallel, BMP-2, Runx2, ALP, OCN and OPN protein levels were much lower in the MOD, which was dramatically raised by naringin at 300mg/kg and 600 mg/kg respectively ( $P < 0.05$  for L-Nar vs MOD and  $P < 0.01$  for H-Nar vs MOD, Figure 7). On the contrary, the PPAR $\gamma$ 2 protein level was down-regulated in response to the ascending dosages of naringin ( $P < 0.05$  for L-Nar vs MOD and  $P < 0.01$  for H-Nar vs MOD, Figure 7). This implied that naringin may increase the osteogenic rather than adipogenic potential of BMSCs dose-dependently.

**Discussion**

SONFH is a devastating and irreversible disease following steroid therapy. Several postulations explain the pathogenesis including abnormal lipid metabolism, oxidative stress, genetic tendency and so forth, but the underlying

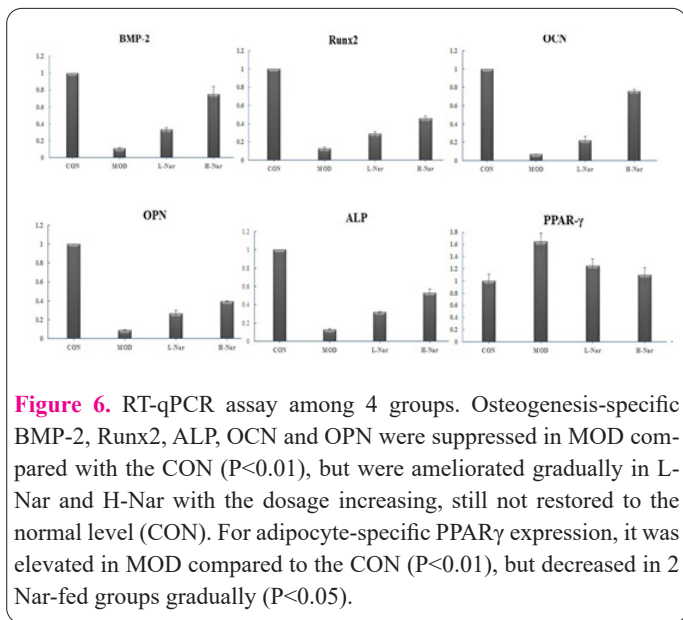


**Figure 6.** RT-qPCR assay among 4 groups. Osteogenesis-specific BMP-2, Runx2, ALP, OCN and OPN were suppressed in MOD compared with the CON ( $P < 0.01$ ), but were ameliorated gradually in L-Nar and H-Nar with the dosage increasing, still not restored to the normal level (CON). For adipocyte-specific PPAR $\gamma$  expression, it was elevated in MOD compared to the CON ( $P < 0.01$ ), but decreased in 2 Nar-fed groups gradually ( $P < 0.05$ ).

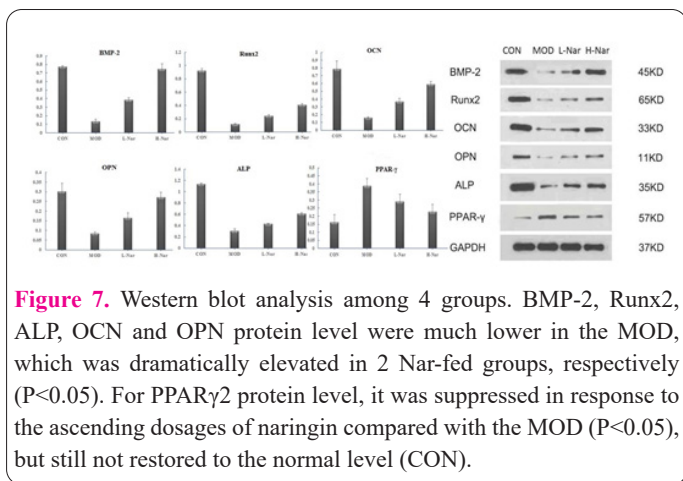


**Figure 7.** Western blot analysis among 4 groups. BMP-2, Runx2, ALP, OCN and OPN protein level were much lower in the MOD, which was dramatically elevated in 2 Nar-fed groups, respectively ( $P < 0.05$ ). For PPAR $\gamma$ 2 protein level, it was suppressed in response to the ascending dosages of naringin compared with the MOD ( $P < 0.05$ ), but still not restored to the normal level (CON).

mechanism remains unveiled. Various medical agents have been introduced for preventing the development of SONFH at an early stage for decades, but their adverse reactions have become a major concern with limited efficacy and safety (9). Recently citrus flavanone naringin has garnered great interest due to its non-toxic nature with fewer side effects than synthetic drugs. It possesses a wide range of pharmacological activities for various diseases including cardiovascular disease, diabetes mellitus, metabolic syndrome, neurodegeneration, hepatic injury, renal damage, osteoporosis and cancer (54). No death, weight loss or other symptoms after naringin treatment in our evaluation revealed that naringin abrogated LPS-induced inflammation. The reduction of LPS-induced GPT elevation showed no adverse effect on the liver. Meantime, naringin may reduce the risk of early-stage ON compared to the MOD group, but still 61.1% and 22.2% of Nar-fed rats developed ON. No obvious difference in ON extent among the three groups suggested that there may be a threshold beyond which ON was initiated, even if the prophylactic treatment was given. Naringin would not prevent ON progression once the threshold was reached, which resembled Motomura G's findings (10).

The primary ON pathogenesis is abnormal lipid metabolism including elevated adipogenesis, extravascular lipid deposits and intravascular hyperlipidaemia. On one hand, marrow adipogenesis is synchronized with steroid-induced bone resorption and is typical of a significant

increase in the number (hyperplasia) and size (hypertrophy) of marrow adipocytes (55). This was evidenced by an obvious reduction of femoral BMD and elevated adipocyte parameters in MOD histology. Moreover, the adipocyte-specific PPAR $\gamma$ 2 acted as an essential mediator of osteoclastogenesis (18,56,57). Wan reported that PPAR $\gamma$  activation in vivo promoted osteoclast-mediated bone resorption in a receptor-dependent manner (58). But naringin could raise femoral BMD and inhibit adipogenesis by progressively decreasing PPAR $\gamma$ 2 expression in the two groups compared to the MOD group. On the other hand, extravascular lipid deposits accompany a high level of lipid transport. A high LDL/HDL cholesterol ratio is considered to reflect the level of lipid transport to the peripheral tissues (10,59). Such lipid transport may be predictive of interosseous lipid deposition, which has been suggested to be a risk factor for human ON (60). It should be noted that a high LDL/HDL ratio does not correspond to a high serum level of cholesterol, since the serum level of cholesterol reflects the total delivery to and from the peripheral tissues. But significant lipid transport resulting from a high LDL/HDL ratio may have led to at least a local (interosseous) hyperlipidaemic state in rat ON lesions, as supported by elevated adipocyte parameters in this study, as well as other clinical and experimental studies of ON (61,62). Our data showed that naringin not only attenuated such lipid transport to peripheral tissues but also inhibited interosseous excessive lipid deposits, as evidenced by the naringin-induced decrease in LDL/HDL ratio and adipocyte parameters. Recent studies have suggested that naringin lowers the plasma lipid levels by suppressing hepatic fatty acid synthase, glucose-6-phosphate dehydrogenase, HMG-CoA reductase, acyl CoA/cholesterol acyltransferase activities and by increasing fecal fat (63). The hypolipidaemic activity of naringin could be also due to its antioxidant potential. Structurally, naringin possesses -OH groups which could contribute to its potent antioxidant and free radical scavenging activities. This potential indirectly decreased the lipid profiles by mitigating the free radical-mediated lipid peroxidation in steroid-induced oxidative stress (64).

There is a consensus that bone ischemia results not only from intraosseous hypertension because of extravascular lipid deposition and elevation of adipogenesis but from intravascular hyperlipidaemia-induced disturbances of the coagulation-fibrinolysis system in the femoral head (62). Hyperlipidaemia has been postulated to be partly responsible for endothelial perturbation, resulting in a prothrombotic state (65). Jones proposed a fat embolization theory whereby hyperlipidaemia might accelerate the abnormalities in the blood coagulation system, triggering thrombi or lipid emboli and microvascular occlusion (66). Then two indices including APTT and t-PA/PAI-I were adopted in our study for assessing the abnormal coagulopathy induced by the steroid. APTT is an index of coagulation, while t-PA/PAI-I reflected the balance between anti-fibrinolysis and pro-fibrinolysis (13,59). The significant decrease in APTT and tPA/PAI-I levels in the MOD at week 1 resembled the previous findings in steroid-induced ON (13), suggesting the hypercoagulable and hypofibrinolytic states in blood vessels related closely to ON occurrence. Naringin could dose-dependently counteract both hypercoagulation and hypofibrinolysis by the gradual increase of APTT and t-PA/PAI-I in the naringin groups

compared to the MOD group in its early stage.

Recently, oxidative stress as a major underlying reason for SONFH has received more attention because it's involved in the above-mentioned events. Accumulation of lipid peroxidative products and oxidative DNA damage in the bone occurs shortly after steroid application and before ON occurrence. For BMSCs, oxidative stress is regarded as a crucial mediator for steroid-induced adipogenesis (67). Moreover, oxidative stress is identified as an important mechanism contributing to endothelium injury (45). These events enhanced coagulability, predisposing to thrombosis and may cause further damage to blood vessels. This stress indulges in endothelial dysfunction due to steroid-induced imbalance between excessive oxidants, such as reactive oxygen species (ROS) and free radicals, and suppression of the antioxidant defenses, especially glutathione (GSH). Pathological ROS production is reckoned as the direct cause of oxidative damage to endothelial function, and free radicals initiate lipid peroxidation which has been implicated in various tissue injuries (68). GSH is a principal endogenous antioxidant that provides the major defense against endothelial injury by inhibiting the increase in lipid peroxide (LPO), whereas LPO is a biochemical indicator of tissue injury by ROS and free radicals (69,70). Ichiseki et al. (45) found that GSH significantly decreased while LPO increased in the early stage of rabbit SONFH, indicative of oxidative damage which impaired vascular permeability. Similar changes could also be found in the MOD at week 1 post-induction. Hence, GSH/LPO in plasma is a biochemical marker showing the level of oxidative stress in the early stage of ON. The other marker TM is a cell surface glycoprotein that is mainly expressed in endothelial cells and resists both hypercoagulation and hypofibrinolysis after endothelial cell injury (34). Thus TM in plasma is an index of endothelial injury. The close correlation between GSH/LPO and TM ( $\rho=0.843$ ) in the MOD at week 1 post-induction strongly suggested that activated oxidative stress was indeed involved in an endothelial injury at the early stage. Our data implied that naringin was able to protect the endothelium from oxidative injury by progressive amelioration of GSH/LPO and TM in a dose-related pattern compared to MOD. In view of the importance of angiogenesis in the growth and development of bone, microvessel density was higher in naringin groups than in MOD, revealing that naringin could enhance femoral head neovascularization through its antioxidant and hypolipidaemic actions.

Concurrently, the above-mentioned events may trigger multiple vicious signaling pathways and eventually attribute to the differentiation of BMSCs into adipocytes rather than osteoblasts. There are many signaling pathways involved in promoting osteogenic and/or adipogenic lineage differentiation of BMSCs, of which the two most important are BMP2/Runx2 and PPAR $\gamma$  signaling pathways (71). As such, diverting improper differentiation of BMSCs relies on the dual regulations of naringin via the 2 pivotal pathways, as assessed by expression of the specific markers: ALP activity, calcium nodules as well as the related gene and protein expression. Following previous studies, naringin can rescue the ALP activity and mineralization in impaired BMSCs, i.e. early and later phases of osteogenic differentiation (16). Moreover, steroid-repressed mRNA and protein expression of BMP-2 and Runx2 was up-regulated by naringin as well as other

crucial markers ALP, OCN and OPN. Runx2 is at the node of many signaling pathways regulating osteoblast differentiation and is regulated by BMP-2 (72). ALP, which is expressed during the post-proliferative period of extracellular matrix maturation, has been widely recognized as an early marker for osteoblast differentiation (73). Moreover, OCN and OPN which occur later (73), have also been used as markers of osteoblastic activity. Our findings showed that naringin was involved in the BMP2/Runx2 signaling pathway in the osteogenic differentiation and maturation of BMSCs. New bone formation in the focal area in response to various doses of naringin fit with the osteogenic changes in cell cultures. Likewise, the parallel increases in adipocyte parameters and expression level of PPAR $\gamma$ 2 in the MOD supported the central role of PPAR $\gamma$ 2 in adipogenesis, because no factor has yet been identified that can induce normal adipogenesis in its absence (51). All critical cell signaling pathways involved in adipogenesis converge on PPAR $\gamma$  and most factors that stimulate adipogenesis ultimately exert their effect through the regulation of this transcription factor (51). Hence, naringin responds to steroids in a dose-dependent fashion by prompting BMP2/Runx2 and inhibiting PPAR $\gamma$  signaling pathways. But the interactive mechanism of Runx2 and PPAR $\gamma$  with naringin as the transcriptional co-activator of both factors remains ill-defined.

PPAR $\gamma$  is a widespread ligand-activated nuclear transcription receptor known to play a role in normal cell function. It is not only a key regulator of lipid metabolism and vasculogenesis but also emerging as an important regulator of the response to oxidative stress and inflammation (73). But PPAR $\gamma$  has tissue-specific requirements for its regulations (74). PPAR $\gamma$  activation by naringin can exert antioxidant and anti-inflammatory effects in pancreatic  $\beta$ -cells, hepatocytes and glomeruli of type 2 diabetic rats (63). Evidences of naringin as a potential treatment for alcoholism and Huntington disease also showed that naringin improved neural PPAR $\gamma$  levels to protect neurons from inflammation, apoptosis and oxidative stress (75,76). Since PPAR $\gamma$  is a master regulator of adipogenesis, normal bone physiology needs a low level of PPAR $\gamma$  expression (77). As PPAR $\gamma$  has a high affinity for steroid receptors (77), pathologic upregulation of PPAR $\gamma$  by steroids may be implicated in ON pathophysiology by regulating multiple pathways of apoptosis, lipid metabolism disorder, oxidative stress, endothelial damage and so on (78). Those pathways are interrelated and form a complicated signal transmission network that cannot be blocked easily once initiated by PPAR $\gamma$  overexpression. Some studies of human PPAR $\gamma$  gene polymorphisms confirmed the genetic- or pharmacologically-induced alterations in PPAR $\gamma$  cause patient-specific sensitivity to steroids (77). Our findings showed that naringin antagonized PPAR $\gamma$  expression and subsequent BMSC adipogenesis with a concomitant agitation in the Runx2 pathway. Therefore, PPAR $\gamma$  might be a pathologic switch or useful target whereby steroid creates an ON susceptibility or naringin stops the subsequent vicious cycle from ever starting.

Currently, many studies have focused on the treatment dosages of naringin administered in vitro and in vivo. Concerning its toxic effects, it is reported that naringin is safe and produced no lethality at a very high dose (5000 mg/kg, by mouth) in mice (79). Moreover, Lambev et al. demonstrated that LD50 of naringin by the ip route in the

rat and guinea pig is 2000 mg/kg (80). Not all concentrations of naringin were effective at enhancing the proliferation and osteogenic differentiation of BMSCs in cell cultures (53). The best doses used in animal models varied from 40 mg/kg to 7g/kg (39) with no consideration of endogenous PPAR $\gamma$  levels representing different pathologic conditions. As a natural ligand of PPAR $\gamma$  (75), naringin may act as a selective PPAR $\gamma$  modulator (74), in which agonism for the receptor is achieved in one tissue while partial agonism or even antagonism occurs in another tissue based on endogenous PPAR $\gamma$  expression level. This modulation of naringin is similar to its double-directional adjusting function of estrogenic or anti-estrogenic activities in treating osteoporosis (81). At low concentrations or lack of endogenous estrogen, the phytoestrogen naringin showed estrogenic agonist activity while it also acted as an estrogenic antagonist at high concentrations or too much endogenous estrogen. Therefore, in the face of excessive endogenous PPAR $\gamma$  in SONFH, only high doses of naringin such as 300mg/kg or 600mg/kg in our study can stop PPAR $\gamma$ -mediated adipogenesis and prompt BMP2/Runx2 signaling pathways.

The current study has several limitations. Firstly, the optimal dosing and time-dependent effects of naringin on SONFH shall be further undertaken by observation of endogenous PPAR $\gamma$  levels. Secondly, the detailed molecular research would endeavor to investigate the antagonizing interactions between the naringin- and steroid-regulated signaling pathways of lipid metabolism, inflammation, apoptosis, and endothelial damage. Otherwise, more details about the effect of naringin on steroid-induced oxidative stress need to be elucidated by assessing the antioxidant enzyme and lipid-metabolizing enzyme activities during ON progression. Meanwhile,  $\mu$ CT-based angiography and angiogenesis-related gene and protein expression at the examined sites should be applied for further exploration of naringin as a selective PPAR $\gamma$  modulator in protecting the endothelium from impairment by the steroid.

In summary, the genesis and progression of SONFH are complicated processes affected by multiple factors and signaling pathways, forming a vicious cycle targeting osteoblast death or apoptosis. The pleiotropic actions of naringin appear to satisfy the need for withstanding the above pathogenic mechanisms of SONFH, eventually relying on dual regulations of BMP2/Runx2 and PPAR $\gamma$  signaling pathways. Taken with the present findings and previous reports of its benefits as well as its safety, it appears that naringin could be a potential promising novel agent of natural origin for SONFH, either alone or as an adjunct to improve the efficacy of existing medications in pharmacotherapy.

### Acknowledgments

This work was supported by the Shandong Science and Technology Development Project (2011WSB 26023).

### References

1. Mont MA, Cherian JJ, Sierra RJ, Jones LC, Lieberman JR. Nontraumatic osteonecrosis of the femoral head: Where do we stand today? A ten-year update. *J Bone Joint Surg Am* 2015; 97(19): 1604-1627. <https://doi.org/10.2106/JBJS.O.00071>
2. Kuroda Y, Matsuda S, Akiyama H. Joint-preserving regenerative therapy for patients with early-stage osteonecrosis of the femo-

- ral head. *Inflamm Regen* 2016; 36: 4. <https://doi.org/10.1186/s41232-016-0002-9>
3. van der Jagt D, Mokete L, Pietrzak J, Zalavras CG, Lieberman JR. Osteonecrosis of the femoral head: evaluation and treatment. *JAAOS-Journal of the American Academy of Orthopaedic Surgeons* 2015; 23(2): 69-70. <https://doi.org/10.5435/JAAOS-D-14-00431>
  4. Cui L, Zhuang Q, Lin J, Jin J, Zhang K, Cao L, Lin J, Yan S, Guo W, He W, Pei F, Zhou Y, Weng X. Multicentric epidemiologic study on six thousand three hundred and ninetyfive cases of femoral head osteonecrosis in China. *Int orthop* 2016; 40(2): 267-276. <https://doi.org/10.1007/s00264-015-3061-7>
  5. Kubo T, Ueshima K, Saito M, Ishida M, Arai Y, Fujiwara H. Clinical and basic researchon steroid-induced osteonecrosis of the femoral head in Japan. *J Orthop Sci* 2016; 21(4): 407-413. <https://doi.org/10.1016/j.jos.2016.03.008>
  6. Powell C, Chang C, Naguwa SM, Cheema G, Gershwin ME. Steroid induced osteonecrosis: An analysis of steroid dosing risk. *Autoimmun Rev* 2010; 9(11): 721-743. <https://doi.org/10.1016/j.autrev.2010.06.007>
  7. Fang SH, Li YF, Jiang JR, Chen P. Relationship of  $\alpha$ 2-macroglobulin with steroid-induced femoral head necrosis: A Chinese population-based association study in Southeast China. *Orthop Surg* 2019; 11(3): 481-486. <https://doi.org/10.1111/os.12492>
  8. Drescher W, Schlieper G, Floege J, Eitner F. Steroid-related osteonecrosis-an update. *Nephrol Dial Transplant* 2011; 26(9): 2728-2731. <https://doi.org/10.1093/ndt/gfr212>
  9. Yoon BH, Jones LC, Chen CH, Cheng EY, Cui Q, Drescher W, Fukushima W, Gangji V, Goodman SB, Ha YC, Hernigou P, Hungerford M, Iorio R, Jo WL, Khanduja V, Kim H, Kim SY, Kim TY, Lee HY, Lee MS, Lee YK, Lee YJ, Mont MA, Sakai T, Sugano N, Takao M, Yamamoto T, Koo KH. Etiologic classification criteria of ARCO on femoral head osteonecrosis Part 1: Glucocorticoid-associated osteonecrosis. *J Arthroplasty* 2019; 34(1): 163-168. <https://doi.org/10.1016/j.arth.2018.09.005>
  10. Motomura G, Yamamoto T, Irisa T, Miyanishi K, Nishida K, Iwamoto Y. Dose effects of corticosteroids on the development of osteonecrosis in rabbits. *J Rheumatol* 2008; 35(12): 2395-2399. <https://doi.org/10.3899/jrheum.080324>
  11. Li X, Jin L, Cui Q, Wang GJ, Balian G. Steroid effects on osteogenesis through mesenchymal cell gene expression. *Osteoporos Int* 2005; 16(1): 101-108. <https://doi.org/10.1007/s00198-004-1649-7>
  12. Ueda S, Ichiseki T, Yoshitomi Y, Yonekura H, Ueda Y, Kaneuji A, Matsumoto T. Osteocytic cell necrosis is caused by a combination of glucocorticoid-induced Dickkopf-1 and hypoxia. *Med Mol Morphol* 2015; 48(2): 69-75. <https://doi.org/10.1007/s00795-014-0077-9>
  13. Glueck CJ, Freiberg RA, Wang P. Heritable thrombophilia-hypofibrinolysis and osteonecrosis of the femoral head. *Clin Orthop Relat Res* 2008; 466(5): 1034-1040. <https://doi.org/10.1007/s11999-008-0148-0>
  14. Calder JD, BATTERY L, Revell PA, Pearse M, Polak JM. Apoptosis: a significant cause of bone cell death in osteonecrosis of the femoral head. *J Bone Joint Surg Br* 2004; 86(8): 1209-1213. <https://doi.org/10.1302/0301-620x.86b8.14834>
  15. Lin L, Dai SD, Fan GY. Glucocorticoid-induced differentiation of primary cultured bone marrow mesenchymal cells into adipocytes is antagonized by exogenous Runx2. *APMIS* 2010; 118(8): 595-605. <https://doi.org/10.1111/j.1600-0463.2010.02634.x>
  16. Wu F, Jiao J, Liu F, Yang Y, Zhang S, Fang Z, Dai Z, Sun Z. Hypermethylation of Frizzled1 is associated with Wnt/ $\beta$ -catenin signaling inactivation in mesenchymal stem cells of patients with steroid-associated osteonecrosis. *Exp Mol Med* 2019; 51(2): 1-9. <https://doi.org/10.1038/s12276-019-0220-8>
  17. Tao SC, Yuan T, Rui BY, Zhu ZZ, Guo SC, Zhang CQ. Exosomes derived from human platelet-rich plasma prevent apoptosis induced by glucocorticoid-associated endoplasmic reticulum stress in rat osteonecrosis of the femoral head via the Akt/Bad/Bcl-2 signal pathway. *Theranostics* 2017; 7(3): 733-750. <https://doi.org/10.7150/thno.17450>
  18. Gangji V, Soyfoo MS, Heuschling A, Afzali V, Moreno-Reyes R, Rasschaert J, Gillet C, Fils JF, Hauzeur JP. Non traumatic osteonecrosis of the femoral head is associated with low bone mass. *Bone* 2018; 107: 88-92. <https://doi.org/10.1016/j.bone.2017.11.005>
  19. Hernigou P, Trousselier M, Roubineau F, Bouthors C, Chevalier N, Rouard H, Flouzat-Lachaniette CH. Stem cell therapy for the treatment of hip osteonecrosis: a 30-year review of progress. *Clin Orthop Surg* 2016; 8(1): 1-8. <https://doi.org/10.4055/cios.2016.8.1.1>
  20. Sadile F, Bernasconi A, Russo S, Maffulli N. Core decompression versus other joint preserving treatments for osteonecrosis of the femoral head: a meta-analysis. *Br Med Bull* 2016; 118(1): 33-49. <https://doi.org/10.1093/bmb/ldw010>
  21. Pierce TP, Jauregui JJ, Elmallah RK, Lavernia CJ, Mont MA, Nace J. A current review of core decompression in the treatment of osteonecrosis of the femoral head. *Curr Rev Musculoskelet Med* 2015; 8(3): 228-232. <https://doi.org/10.1007/s12178-015-9280-0>
  22. Al Omran A. Multiple drilling compared with standard core decompression for avascular necrosis of the femoral head in sickle cell disease patients. *Arch Orthop Trauma Surg* 2013; 133(5): 609-613. <https://doi.org/10.1007/s00402-013-1714-9>
  23. Bae JY, Kwak DS, Park KS, Jeon I. Finite element analysis of the multiple drilling technique for early osteonecrosis of the femoral head. *Ann Biomed Eng* 2013; 41(12): 2528-2537. <https://doi.org/10.1007/s10439-013-0851-1>
  24. Yamamoto T, Motomura G, Karasuyama K, Nakashima Y, Doi T, Iwamoto Y. Results of the Sugioka transtrochanteric rotational osteotomy for osteonecrosis: Frequency and role of a defect of the quadratus femoris muscle in osteonecrosis progression. *Orthop Traumatol Surg Res* 2016; 102(3): 387-390. <https://doi.org/10.1016/j.otsr.2016.01.017>
  25. Zhao G, Yamamoto T, Ikemura S, Motomura G, Mawatari T, Nakashima Y, Iwamoto Y. Radiological outcome analysis of transtrochanteric curved varus osteotomy for osteonecrosis of the femoral head at a mean follow-up of 12.4 years. *J Bone Joint Surg Br* 2010; 92(6): 781-786. <https://doi.org/10.1302/0301-620X.92B6.23621>
  26. Shah SN, Kapoor CS, Jhaveri MR, Golwala PP, Patel S. Analysis of outcome of avascular necrosis of femoral head treated by core decompression and bone grafting. *J Clin Orthop Trauma* 2015; 6(3): 160-166. <https://doi.org/10.1016/j.jcot.2015.03.008>
  27. Pierce TP, Elmallah RK, Jauregui JJ, Poola S, Mont MA, Delanois RE. A current review of non-vascularized bone grafting in osteonecrosis of the femoral head. *Curr Rev Musculoskelet Med* 2015; 8(3): 240-245. <https://doi.org/10.1007/s12178-015-9282-y>
  28. Fontecha CG, Roca I, Barber I, Menendez ME, Collado D, Mascarenhas VV, Barrera-Ochoa S, Soldado F. Femoral head bone viability after free vascularized fibular grafting for osteonecrosis: SPECT/CT study. *Microsurgery* 2016; 36(7): 573-577. <https://doi.org/10.1002/micr.22452>
  29. Pakos EE, Megas P, Paschos NK, Syggelos SA, Kouzelis A, Georgiadis G, Xenakis TA. Modified porous tantalum rod technique for the treatment of femoral head osteonecrosis. *World J Orthop* 2015; 6(10): 829-837. <https://doi.org/10.5312/wjo.v6.i10.829>
  30. Wright JG, Einhorn TA, Heckman JD. Grades of recommendation. *J Bone Joint Surg Am* 2005; 87(9): 1909-1910. <https://doi.org/10.1007/s10439-013-0851-1>

- org/10.2106/JBJS.8709.edit
31. Chughtai M, Piuzzi NS, Khlopas A, Jones LC, Goodman SB, Mont MA. An evidence-based guide to the treatment of osteonecrosis of the femoral head. *Bone Joint J* 2017; 99-B(10): 1267-1279. <https://doi.org/10.1302/0301-620X.99B10.BJJ-2017-0233.R2>
  32. Lee YJ, Cui QJ, Koo KH. Is there a role of pharmacological treatments in the prevention or treatment of osteonecrosis of the femoral head?: a systematic review. *J Bone Metab* 2019; 26(1): 13-18. <https://doi.org/10.11005/jbm.2019.26.1.13>
  33. Li F, Sun X, Ma J, Ma X, Zhao B, Zhang Y, Tian P, Li Y, Han Z. Naringin prevents ovariectomy-induced osteoporosis and promotes osteoclasts apoptosis through the mitochondria-mediated apoptosis pathway. *Biochem Biophys Res Commun* 2014; 452(3): 629-635. <https://doi.org/10.1016/j.bbrc.2014.08.117>
  34. Zhang G, Qin L, Sheng H, Wang XL, Wang YX, Yeung DK, Griffith JF, Yao XS, Xie XH, Li ZR, Lee KM, Leung KS. A novel semisynthesized small molecule icaritin reduces incidence of steroid-associated osteonecrosis with inhibition of both thrombosis and lipid-deposition in a dose-dependent manner. *Bone* 2009; 44(2): 345-356. <https://doi.org/10.1016/j.bone.2008.10.035>
  35. Lv J, Sun X, Ma J, Ma X, Xing G, Wang Y, Sun L, Wang J, Li F, Li Y. Involvement of periostin-sclerostin-Wnt/ $\beta$ -catenin signaling pathway in the prevention of neurectomy-induced bone loss by naringin. *Biochem Biophys Res Commun* 2015; 468(4): 587-593. <https://doi.org/10.1016/j.bbrc.2015.10.152>
  36. Lavrador P, Gaspar VM, Mano JF. Bioinspired bone therapies using naringin: applications and advances. *Drug Discovery Today* 2018; 23(6): 1293-1304. <https://doi.org/10.1016/j.drudis.2018.05.012>
  37. Hung TY, Chen TL, Liao MH, Ho WP, Liu DZ, Chuang WC, Chen RM. *Drynaria fortunei* J. Sm. promotes osteoblast maturation by inducing differentiation-related gene expression and protecting against oxidative stress-induced apoptotic insults. *J Ethnopharmacol* 2010; 131(1): 70-71. <https://doi.org/10.1016/j.jep.2010.05.063>
  38. Kandhare AD, Ghosh P, Bodhankar SL. Naringin, a flavanone glycoside, promotes angiogenesis and inhibits endothelial apoptosis through modulation of inflammatory and growth factor expression in diabetic foot ulcer in rats. *Chem Biol Interact* 2014; 219: 101-112. <https://doi.org/10.1016/j.cbi.2014.05.012>
  39. Zhao Z, Ma X, Ma J, Sun X, Li F, Lv J. Naringin enhances endothelial progenitor cell (EPC) proliferation and tube formation capacity through the CXCL12/CXCR4/PI3K/Akt signaling pathway. *Chem Biol Interact* 2018; 286: 45-51. <https://doi.org/10.1016/j.cbi.2018.03.002>
  40. Li N, Jiang Y, Wooley PH, Xu Z, Yang SY. Naringin promotes osteoblast differentiation and effectively reverses ovariectomy-associated osteoporosis. *J Orthop Sci* 2013; 18(3): 478-485. <https://doi.org/10.1007/s00776-013-0362-9>
  41. Ang ES, Yang X, Chen H, Liu Q, Zheng MH, Xu J. Naringin abrogates osteoclastogenesis and bone resorption via the inhibition of RANKL-induced NF- $\kappa$ B and ERK activation. *FEBS Lett* 2011; 585(17): 2755-2762. <https://doi.org/10.1016/j.febslet.2011.07.046>
  42. Kerachian MA, Harvey EJ, Cournoyer D, Chow TY, Nahal A, Séguin C. A rat model of early stage osteonecrosis induced by glucocorticoids. *J Orthop Surg Res* 2011; 6: 62. <https://doi.org/10.1186/1749-799X-6-62>
  43. Ma X, Lv J, Sun X, Ma J, Xing G, Wang Y, Sun L, Wang J, Li F, Li Y, Zhao Z. Naringin ameliorates bone loss induced by sciatic neurectomy and increases Semaphorin 3A expression in denervated bone. *Sci Rep* 2016; 6: 24562. <https://doi.org/10.1038/srep24562>
  44. Benson RE, Catalfamo JL, Dodds WJ. A multispecies enzyme-linked immunosorbent assay for von Willebrand's factor. *J Lab Clin Med* 1992; 119(4): 420-427.
  45. Ichiseki T, Matsumoto T, Nishino M, Kaneuji A, Katsuda S. Oxidative stress and vascular permeability in steroid-induced osteonecrosis model. *J Orthop Sci* 2004; 9(5): 509-515. <https://doi.org/10.1007/s00776-004-0816-1>
  46. Mohebbati R, Paseban M, Beheshti F, Soukhtanloo M, Shafei MN, Rakhshandeh H, Rad AK. The preventive effects of standardized extract of *Zataria multiflora* and carvacrol on acetaminophen-induced hepatotoxicity in rat: - *Zataria multiflora* and Carvacrol and Hepatotoxicity. *J Pharmacopuncture* 2018; 21(4): 249-257. <https://doi.org/10.3831/KPI.2018.21.028>
  47. Li GW, Chang SX, Fan JZ, Tian YN, Xu Z, He YM. Marrow adiposity recovery after early zoledronic acid treatment of glucocorticoid-induced bone loss in rabbits assessed by magnetic resonance spectroscopy. *Bone* 2013; 52(2): 668-675. <https://doi.org/10.1016/j.bone.2012.11.002>
  48. Li GW, Xu Z, Chang SX, Nian H, Wang XY, Qin LD. Icarin prevents ovariectomy-induced bone loss and lowers marrow adipogenesis. *Menopause* 2014; 21(9): 1007-1016. <https://doi.org/10.1097/GME.0000000000000201>
  49. Habauzit V, Sacco SM, Gil-Izquierdo A, Trzeciakiewicz A, Morand C, Barron D, Pinaud S, Offord E, Horcajada MN. Differential effects of two citrus flavanones on bone quality in senescent male rats in relation to their bioavailability and metabolism. *Bone* 2011; 49(5): 1108-1116. <https://doi.org/10.1016/j.bone.2011.07.030>
  50. Iwakiri K, Oda Y, Kaneshiro Y, Iwaki H, Masada T, Kobayashi A, Asada A, Takaoka K. Effect of simvastatin on steroid-induced osteonecrosis evidenced by the serum lipid level and hepatic cytochrome P4503A in a rabbit model. *J Orthop Sci* 2008; 13(5): 463-468. <https://doi.org/10.1007/s00776-008-1257-z>
  51. Yu WH, Li FG, Chen XY, Li JT, Wu YH, Huang LH, Wang Z, Li P, Wang T, Lahn BT, Xiang AP. PPAR $\gamma$  suppression inhibits adipogenesis but does not promote osteogenesis of human mesenchymal stem cells. *Int J Biochem Cell Biol* 2012; 44(2): 377-384. <https://doi.org/10.1016/j.biocel.2011.11.013>
  52. Xu N, Liu H, Qu F, Fan J, Mao K, Yin Y, Liu J, Geng Z, Wang Y. Hypoxia inhibits the differentiation of mesenchymal stem cells into osteoblasts by activation of Notch signaling. *Exp Mol Pathol* 2013; 94(1): 33-39. <https://doi.org/10.1016/j.yexmp.2012.08.003>
  53. Liu M, Li Y, Yang ST. Effects of naringin on the proliferation and osteogenic differentiation of human amniotic fluid-derived stem cells. *J Tissue Eng Regen Med* 2017; 11(1): 276-284. <https://doi.org/10.1002/term.1911>
  54. Bharti S, Rani N, Krishnamurthy B, Arya DS. Preclinical evidence for the pharmacological actions of naringin: a review. *Planta Med* 2014; 80(6): 437-451. <https://doi.org/10.1055/s-0034-1368351>
  55. Luo P, Gao F, Han J, Sun W, Li Z. The role of autophagy in steroid necrosis of the femoral head: a comprehensive research review. *Int Osteoporos* 2018; 42(7): 1747-1753. <https://doi.org/10.1007/s00264-018-3994-8>
  56. Pengde K, Fuxing P, Bin S, Jing Y, Jingqiu C. Lovastatin inhibits adipogenesis and prevent osteonecrosis in steroid-treated rabbits. *Joint Bone Spine* 2008; 75(6): 696-701. <https://doi.org/10.1016/j.jbspin.2007.12.008>
  57. Hozumi A, Osaki M, Goto H, Sakamoto K, Inokuchi S, Shindo H. Bone marrow adipocytes support dexamethasone-induced osteoclast differentiation. *Biochem Biophys Res Commun* 2009; 382(4): 780-784. <https://doi.org/10.1016/j.bbrc.2009.03.111>
  58. Wan Y, Chong LW, Evans RM. PPAR- $\gamma$  regulates osteoclastogenesis in mice. *Nat Med* 2007; 13(12): 1496-1503. <https://doi.org/10.1038/nm1672>
  59. Glueck CJ, Freiberg RA, Sieve L, Wang P. Enoxaparin prevents progression of stages I and II osteonecrosis of the hip. *Clin Or-*

- thop Relat Res 2005; 435: 164-170. <https://doi.org/10.1097/01.blo.0000157539.67567.03>
60. Miyanishi K, Yamamoto T, Irisa T, Yamashita A, Jingushi S, Noguchi Y, Iwamoto Y. A high low-density lipoprotein cholesterol to high-density lipoprotein cholesterol ratio as a potential risk factor for corticosteroid-induced osteonecrosis in rabbits. *Rheumatology (Oxford)* 2001; 40(2): 196-201. <https://doi.org/10.1093/rheumatology/40.2.196>
  61. Bai H, Chen T, Lu Q, Zhu W, Zhang J. Gene expression profiling of the bone trabecula in patients with osteonecrosis of the femoral head by RNA sequencing. *J Biochem* 2019; 166(6): 475-484. <https://doi.org/10.1093/jb/mvz060>
  62. Jiang Y, Zhang Y, Zhang H, Zhu B, Li P, Lu C, Xu Y, Chen W, Lin N. Pravastatin prevents steroid-induced osteonecrosis in rats by suppressing PPAR $\gamma$  expression and activating Wnt signaling pathway. *Exp Biol Med (Maywood)* 2014; 239(3): 347-355. <https://doi.org/10.1177/1535370213519215>
  63. Sharma AK, Bharti S, Ojha S, Bhatia J, Kumar N, Ray R, Kumari S, Arya DS. Up-regulation of PPAR $\gamma$ , heat shock protein-27 and-72 by naringin attenuates insulin resistance,  $\beta$ -cell dysfunction, hepatic steatosis and kidney damage in a rat model of type 2 diabetes. *Br J Nutr* 2011; 106(11): 1713-1723. <https://doi.org/10.1017/S000711451100225X>
  64. Rathi VK, Das S, Parampalli Raghavendra A, Rao BSS. Naringin abates adverse effects of cadmium-mediated hepatotoxicity: an experimental study using HepG2 cells. *J Biochem Mol Toxicol* 2017; 31(8). <https://doi.org/10.1002/jbt.21915>
  65. Irisa T, Yamamoto T, Miyanishi K, Yamashita A, Iwamoto Y, Sugioka Y, Sueishi K. Osteonecrosis induced by a single administration of low-dose lipopolysaccharide in rabbits. *Bone* 2001; 28(6): 641-649. [https://doi.org/10.1016/s8756-3282\(01\)00460-4](https://doi.org/10.1016/s8756-3282(01)00460-4)
  66. Jones JP Jr. Fat embolism, intravascular coagulation, and osteonecrosis. *Clin Orthop Relat Res* 1993; 292: 294-308.
  67. Sun ZB, Wang JW, Xiao H, Zhang QS, Kan WS, Mo FB, Hu S, Ye SN. Icarin may benefit the mesenchymal stem cells of patients with steroid-associated osteonecrosis by ABCB1-promoter demethylation: a preliminary study. *Osteoporos Int* 2015; 26(1): 187-197. <https://doi.org/10.1007/s00198-014-2809-z>
  68. Ramakrishnan A, Vijayakumar N, Renuka M. Naringin regulates glutamate-nitric oxide cGMP pathway in ammonium chloride induced neurotoxicity. *Biomed Pharmacother* 2016; 84: 1717-1726. <https://doi.org/10.1016/j.biopha.2016.10.080>
  69. Ahmed OM, Hassan MA, Abdel-Twab SM, Abdel Azeem MN. Navel orange peel hydroethanolic extract, naringin and naringenin have anti-diabetic potentials in type 2 diabetic rats. *Biomed Pharmacother* 2017; 94: 197-205. <https://doi.org/10.1016/j.biopha.2017.07.094>
  70. Huang SL, Jiao J, Yan HW. Hydrogen-rich saline attenuates steroid-associated femoral head necrosis through inhibition of oxidative stress in a rabbit model. *Exp Ther Med* 2016; 11(1): 177-182. <https://doi.org/10.3892/etm.2015.2883>
  71. Huang Z, Cheng C, Cao B, Wang J, Wei H, Liu X, Han Y, Yang S, Wang X. Icarin protects against glucocorticoid-induced osteonecrosis of the femoral head in rats. *Cell Physiol Biomech* 2018; 47(2): 694-706. <https://doi.org/10.1159/000490023>
  72. Huang Y, Jin X, Zhang X, Sun H, Tu J, Tang T, Chang J, Dai K. In vitro and in vivo evaluation of akermanite bioceramics for bone regeneration. *Biomaterials* 2009; 30(28): 5041-5048. <https://doi.org/10.1016/j.biomaterials.2009.05.077>
  73. Caglayan C, Temel Y, Kandemir FM, Yildirim S, Kucukler S. Naringin protects against cyclophosphamide-induced hepatotoxicity and nephrotoxicity through modulation of oxidative stress, inflammation, apoptosis, autophagy, and DNA damage. *Environ Sci Pollut Res Int* 2018; 25(21): 20968-20984. <https://doi.org/10.1007/s11356-018-2242-5>
  74. Ahmadian M, Suh JM, Hah N, Liddle C, Atkins AR, Downes M, Evans RM. PPAR $\gamma$  signaling and metabolism: the good, the bad and the future. *Nat Med* 2013; 19(5): 557-566. <https://doi.org/10.1038/nm.3159>
  75. Bahi A, Nurulain SM, Ojha S. Ethanol intake and ethanol-conditioned place preference are reduced in mice treated with the bioflavonoid agent naringin. *Alcohol* 2014; 48(7): 677-685. <https://doi.org/10.1016/j.alcohol.2014.06.008>
  76. Cui J, Wang G, Kandhare AD, Mukherjee-Kandhare AA, Bodhanekar SL. Neuroprotective effect of naringin, a flavone glycoside in quinolinic acid-induced neurotoxicity: Possible role of PPAR- $\gamma$ , Bax/Bcl-2, and caspase-3. *Food Chem Toxicol* 2018; 121: 95-108. <https://doi.org/10.1016/j.fct.2018.08.028>
  77. Wyles CC, Paradise CR, Houdek MT, Slager SL, Terzic A, Behfar A, van Wijnen AJ, Sierra RJ. CORR® ORS Richard A. Brand Award: Disruption in peroxisome proliferator-activated receptor- $\gamma$  (PPARG) increases osteonecrosis risk through genetic variance and pharmacologic modulation. *Clin Orthop Relat Res* 2019; 477(8): 1800-1812. <https://doi.org/10.1097/CORR.0000000000000713>
  78. Tong P, Wu C, Jin H, Mao Q, Yu N, Holz JD, Shan L, Liu H, Xiao L. Gene expression profile of steroid-induced necrosis of femoral head of rats. *Calcif Tissue Int* 2011; 89(4): 271-284. <https://doi.org/10.1007/s00223-011-9516-y>
  79. Alvarez-González I, Madrigal-Bujaidar E, Dorado V, Espinosa-Aguirre JJ. Inhibitory effect of naringin on the micronuclei induced by ifosfamide in mouse, and evaluation of its modulatory effect on the Cyp3a subfamily. *Mutat Res* 2001; 480-481: 171-178. [https://doi.org/10.1016/s0027-5107\(01\)00197-x](https://doi.org/10.1016/s0027-5107(01)00197-x)
  80. Lambev I, Krushkov I, Zheliazkov D, Nikolov N. Antiexsudativen efekt na naringina pri eksperimentalen belodroben otok i peritonit [Antiexudative effect of naringin in experimental pulmonary edema and peritonitis]. *Eksp Med Morfol* 1980; 19(4): 207-212.
  81. Guo D, Wang J, Wang X, Luo H, Zhang H, Cao D, Chen L, Huang N. Double directional adjusting estrogenic effect of naringin from *Rhizoma drynariae* (Gusuibu). *J Ethnopharmacol* 2011; 138(2): 451-457. <https://doi.org/10.1016/j.jep.2011.09.034>